ADVANCED OPTICAL MATERIALS
www.advopticalmat.de

Improving Processability and Efficiency of Resonant TADF Emitters: A Design Strategy

David Hall, Subeesh Madayanad Suresh, Paloma L. dos Santos, Eimantas Duda, Sergey Bagnich, Anton Pershin, Pachaiyappan Rajamalli, David B. Cordes, Alexandra M. Z. Slawin, David Beljonne, Anna Köhler, Ifor D. W. Samuel,* Yoann Olivier,* and Eli Zysman-Colman**

A new design strategy is introduced to address a persistent weakness with resonance thermally activated delayed fluorescence (R-TADF) emitters to reduce aggregation-caused quenching effects, which are identified as one of the key limiting factors. The emitter Mes_3DiKTa shows an improved photoluminescence quantum yield of 80% compared to 75% for the reference DiKTa in 3.5 wt% 1,3-bis(*N*-carbazolyl)benzene. Importantly, emission from aggregates, even at high doping concentrations, is eliminated and aggregation-caused quenching is strongly curtailed. For both molecules, triplets are almost quantitatively upconverted into singlets in electroluminescence, despite a significant (≈0.21 eV) singlet-triplet energy gap (ΔE_{ST}), in line with correlated quantum-chemical calculations, and a slow reverse intersystem crossing. It is speculated that the lattice stiffness responsible for the narrow fluorescence and phosphorescence emission spectra also protects the triplets against nonradiative decay. An improved maximum external quantum efficiencies (EQE_{max}) of 21.1% for Mes_3DIKTa compared to the parent DiKTa (14.7%) and, importantly, reduced efficiency roll-off compared to literature resonance TADF organic light-emitting diodes (OLEDs), shows the promise of this design strategy for future design of R-TADF emitters for OLED applications.

1. Introduction

Thermally activated delayed fluorescence (TADF) permits 100% internal quantum efficiency (IQE) in electroluminescent devices as this mechanism permits conversion of nonradiative triplet excited states to radiative singlet states via reverse intersystem crossing (RISC).[1] RISC is made efficient by having a small energy gap between the lowest triplet and singlet excited states (ΔE_{ST}). The most common molecular design for achieving small ΔE_{ST} in organic emitters is based on a donor–acceptor paradigm where the highest occupied molecular orbital (HOMO) and lowest unoccupied molecular orbital (LUMO) are poorly electronically coupled and usually spatially separated, thus reducing the exchange integral.[2] Conventional donor–acceptor TADF compounds emit from an excited state that is strongly charge transfer (CT) in nature. Generally, these CT emitters have emission spectra that are

D. Hall, Dr. S. M. Suresh, Dr. P. Rajamalli, Dr. D. B. Cordes, Prof. A. M. Z. Slawin, Prof. E. Zysman-Colman
Organic Semiconductor Centre
EaStCHEM School of Chemistry
University of St Andrews
St Andrews KY16 9ST, UK
E-mail: eli.zysman-colman@st-andrews.ac.uk

D. Hall, Dr. A. Pershin, Prof. D. Beljonne, Prof. Y. Olivier
Laboratory for Chemistry of Novel Materials
University of Mons
7000 Mons, Belgium

The ORCID identification number(s) for the author(s) of this article can be found under https://doi.org/10.1002/adom.201901627.

DOI: 10.1002/adom.201901627

Dr. P. L. dos Santos, Dr. P. Rajamalli, Prof. I. D. W. Samuel
Organic Semiconductor Centre
SUPA School of Physics and Astronomy
University of St Andrews
St Andrews KY16 9SS, UK
E-mail: idws@st-andrews.ac.uk

E. Duda, Dr. S. Bagnich, Prof. A. Köhler
Soft Matter Optoelectronics
BIMF & BPI
University of Bayreuth
Universitätsstraße 30, 95447 Bayreuth, Germany
E-mail: anna.koehler@uni-bayreuth.de

Prof. Y. Olivier
Unité de Chimie Physique Théorique et Structurale & Laboratoire de Physique du Solide
Namur Institute of Structured Matter
Université de Namur
Rue de Bruxelles, 61, 5000 Namur, Belgium
E-mail: yoann.olivier@unamur.be

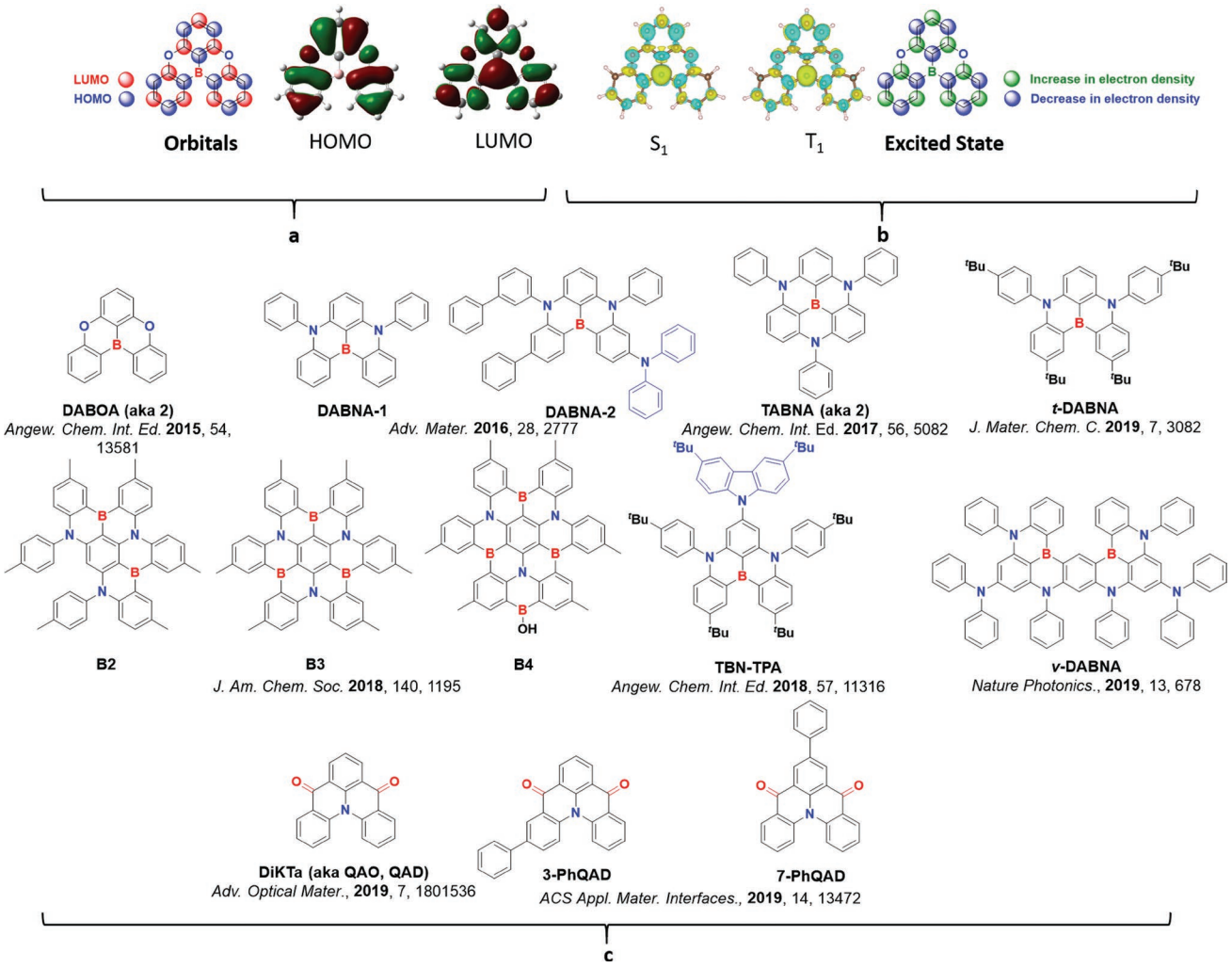

Figure 1. Previously reported R-TADF emitters. a) Simplified resonating HOMO/LUMO plot for DABOA and HOMO-LUMO distributions calculated using density functional theory (DFT); b) simplified difference density plot of DABOA and singlet and triplet difference density plots calculated in the gas phase using spin-component scaling second-order approximate coupled-cluster (SCS-CC2) approach; c) structures of previously reported R-TADF emitters and related photophysical and OLED data.

very broad in nature, with full-width at half-maximum (FWHM), often as high as 100 nm, leading to poor color purity.[3]

In 2015, a new approach for TADF emitters was presented by Hatakeyama and co-workers.[4] Their design involved an alternating HOMO/LUMO pattern based on complimentary resonance effects of electron-donating oxygen and electron-withdrawing boron moieties (**Figure 1**a). The first emitter of this resonating TADF (R-TADF) family, **DABOA** (originally called **2**a, but renamed for clarity), possessed a suitably small ΔE_{ST} of 0.15 eV and a reasonably high photoluminescence quantum yield, Φ_{PL}, of 72% in 1 wt% poly(methyl methacrylate) (PMMA) thin film. In this first report no devices were fabricated as the emission maximum, λ_{PL}, was too high in energy at 399 nm.[4]

Following this initial work, the same group modified their design and incorporated stronger nitrogen-based donor moieties (Figure 1c).[5] Blue-emitting compounds **DABNA-1** and **DABNA-2** (λ_{PL} = 460 and 469 nm, respectively), showing very high Φ_{PL} of 88 and 90%, respectively, in 1 wt% mCBP, were reported. These emitters were incorporated into organic light-emitting diodes (OLEDs), which showed very good maximum external quantum efficiencies (EQE_{max}) of 13.2% and 20.2%, respectively. Though the OLEDs showed very large efficiency roll-off and did not reach a luminance of 1000 cd m^{-2}, **DABNA-2** nevertheless represents one of the most efficient deep blue emitters reported to date with Commission Internationale d'Éclairage (CIE) coordinates of (0.12, 0.13).[6] Building from **DABNA-1**, the C_3-symmetric derivative **TABNA** (originally named **2**, renamed for clarity) likewise showed a similarly small ΔE_{ST} of 0.21 eV along with a reasonable Φ_{PL} of 54% in 1 wt% PMMA films; however, the undesired blueshift in the emission (λ_{PL} = 399 nm) again led to no devices being fabricated.[7] Going beyond the simplistic orbital picture, we demonstrated, based on highly correlated quantum chemical calculations at the spin-component scaling second-order approximate coupled-cluster (SCS-CC2) level of theory, that **DABNA-1** and **TABNA** display short-range charge transfer in both the T_1 and S_1 excited states, which is responsible for their small ΔE_{ST} while maintaining the necessary overlap between

the hole and electron wavefunctions to guarantee a large oscillator strength, *f*, which explains their high observed Φ_{PL}.[3]

Increasing the number of acceptor groups (**B2**, **B3**, and **B4**) stabilized the LUMO energy and led to blueshifted emission with emission maxima, λ_{PL}, of 455, 441, and 450 nm, respectively, in 1 wt% PMMA.[8] Further, an excellent device performance using **B2**, was reported with EQE_{max} values as high as 18%, coupled with a slightly improved efficiency roll-off compared to the devices with the **DABNA** emitters. The next iteration in design involved the introduction of a donor carbazole derivative and solubilizing *tert*-butyl groups about the skeleton of **DABNA-1** (**TBN-TPA**).[9] The addition of the *tert*-butylcarbazole unit did not adversely affect the multiresonance mechanism, with HOMO/LUMO density remaining localized on the **DABNA-1** core and only a slight observed redshift in the emission at 470 nm (λ_{PL} of **DABNA-1** = 460 nm) coupled with an enhanced Φ_{PL} of 98% in toluene (Φ_{PL} of **DABNA-1** = 89% in CH_2Cl_2). The OLED using **TBN-TPA** showed an excellent EQE_{max} of 32.1% and also an improved efficiency roll-off.[9] Another method to improve efficiency roll-off has been proposed recently where a *tert*-butyl analogue of **DABNA-1**, t-**DABNA** (λ_{PL} = 445), was used alongside an assistant TADF dopant **DMAC-DPS**.[10] Improved EQE_{max} values from 25.1% to 31.4% were observed in the assistant dopant device compared to the OLED with no assistant dopant. Vastly improved efficiency roll-off was also observed where the EQE at 100 cd m^{-2} decreased by only 13% in the assistant dopant device compared to 76% in the device without the assistant dopant. Hatakeyama and co-workers[11] recently reported a B/N containing pentacene decorated with peripheral diphenylamines (v-**DABNA**). The deep blue devices reported show outstanding EQE_{max} and very low efficiency roll-off at 100 cd m^{-2} of 34.4% and 5% (EQE_{100} = 32.8%), respectively, at CIE of (0.12,0.11). To the best of our knowledge, these OLEDs are the highest performing deep-blue devices reported to date. The OLEDs also show very high color purity, with a FWHM of 18 nm in a 1 wt% doped device. A summary of all major photophysical data of literature B/N R-TADF based emitters is in Table S1 (Supporting Information).

R-TADF emitters are clearly very promising, with EQE_{max} of up to 30% possible for blue devices, but their most attractive feature is their consistently narrow emission FWHM. The sharper emission profile is particularly attractive as this translates to improved color purity in the device.[12] R-TADF compounds have small ΔE_{ST}, high Φ_{PL}, and small emission FWHM, making them an ideal class of emitter for OLEDs. However, as many of the examples in Figure 1c are highly planar, they are at risk of quenching due to aggregation and/or excimer formation. Further, nearly all are based on a B/N design, which limits the structural diversity and scope of these emitters.

Mes_3DiKTa (**Figure 2**) was designed in order to mitigate the undesirable quenching by aggregation frequently observed in R-TADF emitters. The mesityl groups were chosen as they would (1) adopt an orthogonal conformation and thus not affect the multiresonance mechanism and (2) their steric bulk will inhibit aggregation-caused quenching.[13] **DiKTa**, acting as a reference emitter, and derivatives have been previously reported; however, their potential as TADF emitters was

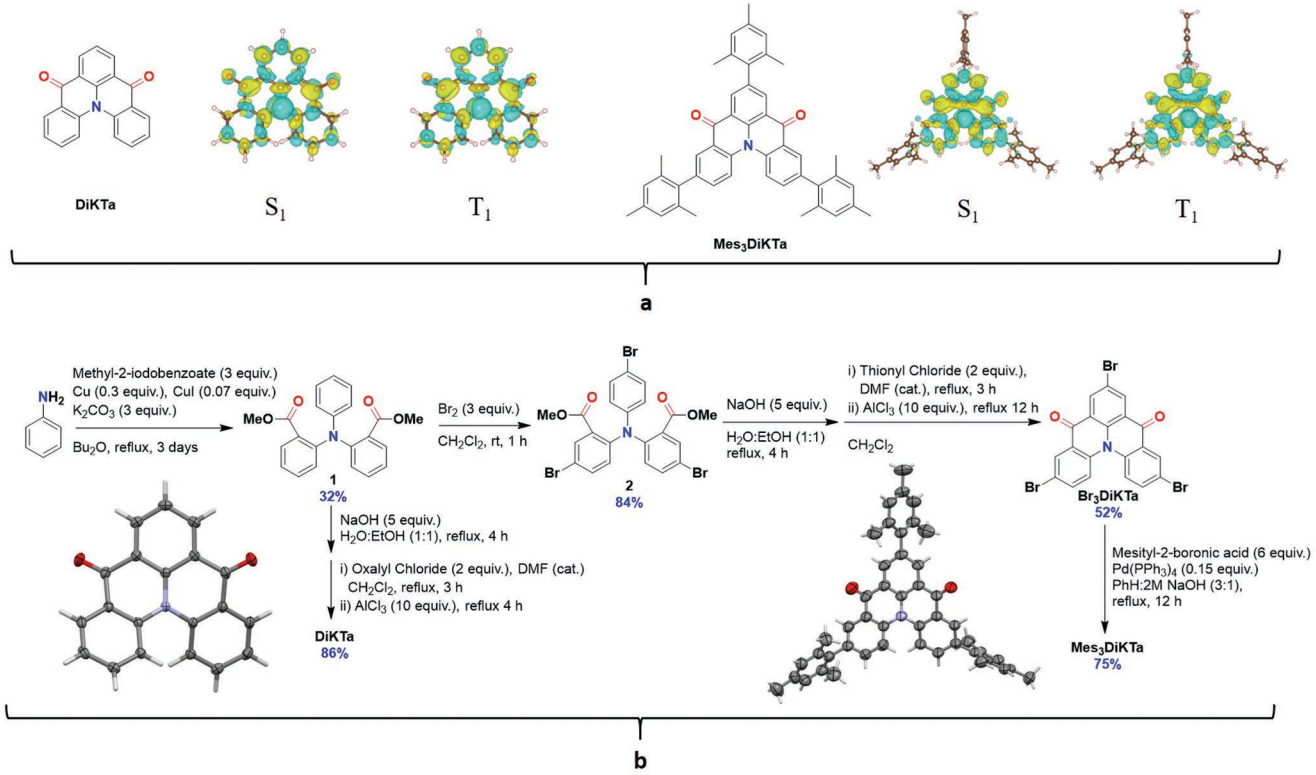

Figure 2. a) Difference density plots of lowest singlet and triplet excited states for **DiKTa** and **Mes_3-DiKTa** calculated in the gas phase using SCS-CC2. Blue indicates an area of decreased electron density while yellow indicates increased electronic density between the ground and excited states. b) Synthesis of **DiKTa** and **Mes_3DiKTa** and ellipsoid plots (50% probability ellipsoids) of the X-ray structure of each emitter.

not identified until very recently, being initially categorized as normal fluorescent emitters.[14] Since commencing our study, **DiKTa** has been reported as a R-TADF emitter under the name of **QAO**.[15] It has a high Φ_{PL} of 72% and narrow blue emission (λ_{PL} = 468 nm; FWHM = 39 nm) in 5 wt% 1,3-bis(*N*-carbazolyl) benzene (mCP), and a high EQE_{max} of 19.4% (at <1 cd m^{-2}). However, the maximum luminance was only 1100 cd m^{-2} and only limited theoretical work was performed. A second emitter in the same report, **QAO-DAd**, is much better described as a donor–acceptor system and showed none of the photophysical characteristics emblematic of R-TADF emitters. In addition, two phenyl substituted derivatives of **DiKTa** were reported, **3-PhQAD** and **7-PhQAD**.[16] Near identical λ_{PL} to **DiKTa** were reported at 466 and 464 nm in 2 wt% mCP, respectively, for **3-PhQAD** and **7-PhQAD** along with comparable Φ_{PL} of 73% and 68%. Addition of the phenyl groups has very little impact upon the photophysics of the **DiKTa** luminophore nor on the device performance where comparable EQE_{max} of 19.1% and 18.7% were reported for **3-PhQAD** and **7-PhQAD**, respectively. The OLED with **7-PhQAD** showed a significant efficiency roll-off with EQE_{100} of 5.4% compared to 10.2% for **3-PhQAD**; however, no explanation was given for this observation. Further, a drop-in luminance compared to the best boron-based R-TADF emitters was observed for **3-PhQAD** (4975 cd m^{-2}) and **7-PhQAD** (2944 cd m^{-2}). There is thus a clear need for improvement in the performance of this new class of R-TADF emitter. Using in silico design and building from our previous work, we demonstrate that peripheral modification of a R-TADF triangulene-type emitter does not affect the R-TADF mechanism, and reduces quenching by aggregation. **Mes_3DiKTa** shows an enhanced Φ_{PL} of 80% compared to 75% for the reference **DiKTa** at 3.5 wt% in mCP. An excellent EQE_{max} of 21.1% at a luminance of 25 cd m^{-2} was obtained, representing the highest for these ketone-based R-TADF emitters. Importantly, improved efficiency roll-off of 31% was also noted with EQE_{100} of 14.5% and a significantly higher maximum luminance of 12 900 cd m^{-2} for the OLED with **Mes_3DiKTa**.

2. Results and Discussion

2.1. Computational Studies

Based on our recent study,[3] all the results presented in the main manuscript are obtained by running higher-level SCS-CC2; for completeness, time-dependent density functional theory (TD-DFT) calculations results are presented in Figure S32 (Supporting Information). All TD-DFT flavors (namely, different functionals and full TD-DFT versus Tamm-Dancoff approximation treatment) lead to different description of both T_1 and S_1 excited states in comparison to SCS-CC2, and also to large overestimations of ΔE_{ST}. Similar to results obtained for **DABNA-1** and **TABNA**, including high-order electronic correlation effects is required to properly account for the short-range charge transfer character in the lowest singlet and triplet excited states of both **DiKTa** and **Mes_3DiKTa**, revealing that the R-TADF mechanism is operative. As expected, there is very little density located on the mesityl groups in **Mes_3DiKTa** (Figure 2). However, the difference density plots show opposite patterns to the previously reported B,N R-TADF emitters because of the inverted design which places a central nitrogen-based donor and peripheral ketone acceptors. In order to further validate our computational methodology and demonstrate its robustness, calculations were performed for each of the literature R-TADF diketone emitters in Figure 1, along with other B,N R-TADF emitters, namely, **DABNA-2**, **t-DABNA**, and **TBN-TPN**. Predicted ΔE_{ST} energies are in good agreement with experiment (Table S9, Supporting Information). We note that our calculations on **3-PhQAD** and **7-PhQAD** sensibly disagree with the interpretation proposed by Zhang and co-workers[16] based on TD-DFT calculations, where the nature of the excited states in these compounds involves CT-LE hybridization, while our SCS-CC2 calculations suggest that T_1 and S_1 are short-range CT excited states.

Calculated ΔE_{ST} for **DiKTa** and **Mes_3DiKTa** are 0.27 and 0.26 eV, respectively, and are expected to be small enough to permit RISC at ambient temperatures. Predicted oscillator strengths, *f*, of 0.20 and 0.23 for each **DiKTa** and **Mes_3DiKTa**, respectively, resulting in k_f of 1.05×10^8 and 1.10×10^8 s^{-1} from S_1 to S_0, which should translate into enhanced Φ_{PL}.

2.2. Synthesis

DiKTa was synthesized using a similar method to that reported previously (Figure 2).[3] Diester, **1** was obtained in modest yield of 32% via a high-temperature Ullmann coupling. The subsequent ring closing reaction produced **DiKTa** in 86% yield. Overall a reduced yield of 26% compared to the original 31% was obtained.[14a] **Mes_3DiKTa** was obtained in good yield following bromination of intermediate **2**, Friedel-Craft acylation to produce brominated **Br_3DiKTa**, and Suzuki-Miyaura coupling with mesityl-2-boronic acid to deliver the target **Mes_3DiKTa**. ^{1}H and ^{13}C NMR, high resolution mass spectrometry, elemental analysis, and high-performance liquid chromatography were used to confirm the structures along with the purity. Single crystal X-ray diffraction data for both emitters indicated different packing motifs; although neither compound shows strong intermolecular interactions, the presence of the mesityl groups does disrupt $\pi\cdots\pi$ interactions in **Mes_3DiKTa** [no centroid$\cdots$centroid distances less than 4.030(3) Å]. The only intermolecular interactions seen in **Mes_3DiKTa** are extremely weak C—H$\cdots\pi$ interactions between a phenyl hydrogen and a mesitylene ring, at distances close to the van der Waals limit (2.85 and 2.06 Å), leading to the formation of weakly interacting molecular stacks along the crystallographic *b*-axis. In **DiKTa** $\pi\cdots\pi$ interactions are found [centroid$\cdots$centroid distance of 3.8793(6) Å] between adjacent emitter molecules, giving rise to interacting stacks running along the *c*-axis (Figure S17, Supporting Information). Good thermal stability was observed with 5% weight loss at 323 and 437 °C for **DiKTa** and **Mes_3DiKTa**, respectively (Figure S29, Supporting Information).

2.3. Optoelectronic Properties

The electrochemical behavior of **DiKTa** and **Mes_3DiKTa** was studied by cyclic voltammetry and differential pulse

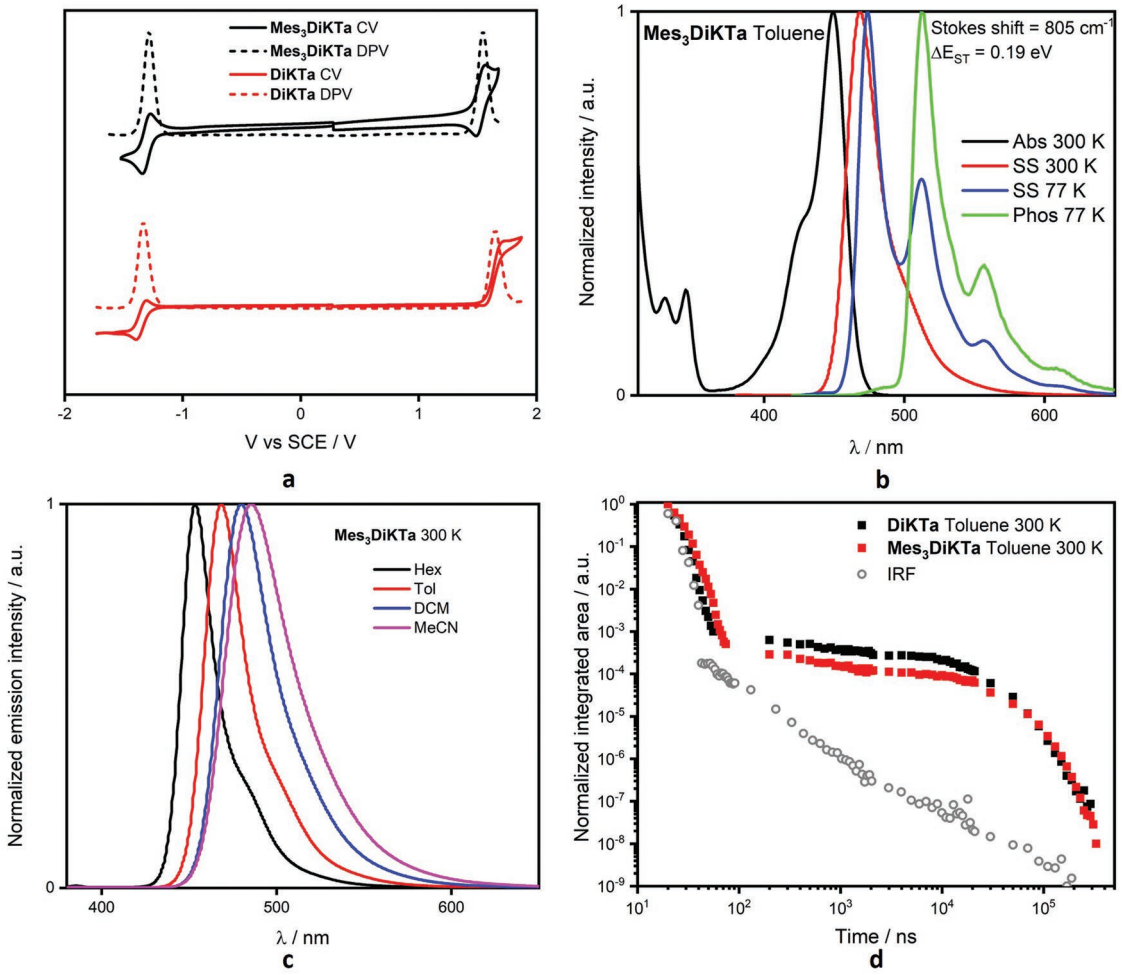

Figure 3. Solution optoelectronic properties. a) Cyclic and differential pulse voltammograms in degassed MeCN with 0.1 M $[nBu_4N]PF_6$ as the supporting electrolyte and Fc/Fc^+ as the internal reference (0.38 V vs SCE).[17] b) Absorption (Abs) and steady-state PL (SS) spectra obtained in toluene at 300 and 77 K, phosphorescence (Phos.) spectra obtained in toluene glass at 77 K after 70 ms delay for 70 ms, λ_{exc} = 415 nm. c) solvatochromatic PL study of Mes_3DiKTa, λ_{exc} = 345 nm. d) Time resolved PL of Mes_3DiKTa and DiKTa in degassed toluene, λ_{exc} = 355 nm detected across the full spectral range, where IRF is the instrument response function.

voltammetry in degassed acetonitrile (MeCN) with tetrabutylammonium hexafluorophosphate as the supporting electrolyte. The cyclic voltammograms (CVs) and differential pulse voltammograms (DPVs) are shown in **Figure 3**a and the data are summarized in Table S3 (Supporting Information). A slightly destabilized HOMO and stabilized LUMO in **Mes_3DiKTa** versus **DiKTa** can be attributed to the mesomeric electron-withdrawing character of the mesityl groups. The reduced $\Delta E_{H\text{-}L}$ in turn is correlated with the observed redshifted emission (vide infra). Further, the mesityl groups contribute to the electrochemical stability of the compound with reversible oxidation and reduction waves by inhibiting an electrochemical degradation process located at the *para*-C—H position to the nitrogen. Atmospheric photoelectron spectroscopy (APS) was also performed on neat films of the emitters to corroborate the HOMO levels inferred from CV (Figure S18, Supporting Information). The APS values are in good agreement with those obtained by DPV (Table S3, Supporting Information). UV–vis spectra in toluene show high-energy, low-intensity bands along with a low-energy high-intensity band, the latter of which we attribute to a short-range charge-transfer S_0–S_1 strongly allowed optical transition typical of multiresonant compounds (Figure 3b and Figure S19, Supporting Information). This is in good agreement with theory, where a high oscillator strength, *f*, of 0.23 and 0.20 for **Mes_3DiKTa** and **DiKTa** is predicted for this transition. A very small positive solvatachromism is observed for this band in the ground state (Figure S19, Supporting Information). This is again consistent with the short-range CT nature of this transition (cf. Tables S4 and S5, Supporting Information).

We next investigated the photophysical properties of the two emitters in toluene. The photoluminescence (PL) spectrum of **Mes_3DiKTa** shows the expected mirror image profile to the absorption spectrum, and the small difference between the peaks of the absorption and emission of 27 nm (805 cm^{-1}) suggests a weak geometry relaxation in the singlet state (Figure 3c and Figure S20a, Supporting Information, for **DiKTa**) highlighting the quite rigid structure of **Mes_3DiKTa** similarly to

DABNA-1; the vibronic progression is less well resolved in the PL spectrum. The rigid nature of the compound is responsible for the narrow emission spectrum at RT. A similar profile but with more pronounced vibronic progression is observed for the phosphorescence spectrum obtained after 70 ms at 77 K in a toluene glass. The ΔE_{ST} of 0.19 eV is sufficiently small to enable a RISC process at room temperature. Modest positive solvatochromism (31 nm, or 1522 cm^{-1} for **DiKTa** and 1408 cm^{-1} for **Mes_3DiKTa**) was observed in the steady-state PL spectra (Figure 3c), in contrast to the larger positive solvatochromism typically observed for conventional D-A TADF emitters.[18] This demonstrates that the nature of the excited states of R-TADF emitters is distinct from conventional D-A TADF emitters. In R-TADF emitters, both T_1 and S_1 are short-range CT excited states, which together with the narrow FWHM of both the fluorescence and the phosphorescence spectra constitute the remarkable characteristics of R-TADF emitters.

Time-resolved PL was measured in both aerated and degassed solutions in toluene. The decays show multiexponential kinetics with both a prompt, τ_p, ns PL lifetime emission and a delayed, τ_d, microsecond PL lifetime. Both **DiKTa** and **Mes_3DiKTa** have a small contribution to the delayed component (Figure 3d), consistent with previous studies of R-TADF emitters,[5] along with τ_d of 33 and 23 µs, respectively. Predicted k_f is larger than experimentally calculated in toluene (1.05×10^8 s^{-1} compared to 4.9×10^7 s^{-1} for **DiKTa** and 1.10×10^8 s^{-1} compared to 5.4×10^7 s^{-1} for **Mes_3DiKTa**), which we attribute to the solvent that tends to stabilize CT-like excitations and reduces their transition dipole moment compared to the gas phase. Solution photophysical data for both emitters in toluene are shown in **Table 1** (the full data for each of the solvents can be found in Tables S4–S6, Supporting Information).

We next investigated the solid-state PL behavior in thin films of 3.5 wt% emitter in mCP (**Table 2**). This concentration was chosen in order to avoid aggregation of the emitters, and mCP was selected as the host matrix as its triplet energy (2.81 eV)[19] is higher than that of the emitters. Promising Φ_{PL} values of 75% and 80% were observed for vacuum-sublimed 3.5 wt% doped films of **DiKTa** and **Mes_3DiKTa**, respectively. To probe whether the higher Φ_{PL} of **Mes_3DiKTa** may result from the suppression of interchromophore interactions by the mesityl groups, we measured the photoluminescence of both materials in mCP as a function of concentration in spin-coated films, which gives slightly lower Φ_{PL} than the vacuum-sublimed ones. **Figure 4**a shows how for a neat film of **DiKTa**, a distinct second, broad peak emerges at about 540 nm, likely resulting from excimer formation, while a neat film of **Mes_3DiKTa** retains its narrow spectral shape. This is accompanied by a strong reduction in Φ_{PL} for **DiKTa** with increasing concentration, while this tails off far more gently for **Mes_3DiKTa** (Figure 4b). Clearly, the introduction of the mesityl groups alleviates close interaction, as was intended by the original chemical design.

Figure 4d shows the time-resolved PL decay traces at different temperatures for **Mes_3DiKTa** in mCP. There is a temperature dependence of the magnitude of the delayed lifetime, τ_d, which expectedly decreases with decreasing temperature from 300 to 200 K (Figure 4d), typical of TADF emitters. The delayed emission we observe at 300 and 200 K is fluorescence from the S_1 state while the emission at 100 and 5 K is phosphorescence from the T_1 state; there is limited delayed fluorescence at these latter two temperatures (Figure S1, Supporting Information). This same behavior is observed for **DiKTa** (Figures S22–S24, Supporting Information). Much like that observed in toluene, the contribution of the delayed emission to the overall emission in **DiKTa** is more prominent than for **Mes_3DiKTa** (Figure S25, Supporting Information), indicating higher TADF emission contribution, possibly associated with the smaller ΔE_{ST} in **DiKTa**.

Figure 4c shows the spectral analysis of the prompt fluorescence at 77 K and phosphorescence (time delay 20 ms) at 77 K for **Mes_3DiKTa** in 3.5 wt% mCP (see Figure S24a, Supporting Information, for **DiKTa**). We were able to estimate the ΔE_{ST} from the onset of these spectra. The slight redshifted emission observed in **Mes_3DiKTa**, for both the S_1 and T_1 states (**Table 3**) versus **DiKTa** can be correlated to the observed smaller electrochemical gap. Good agreement for ΔE_{ST} between experiment and theory is observed, with **DiKTa** (ΔE_{STexp} = 0.20 eV vs $\Delta E_{STtheory}$ = 0.27 eV), while for **Mes_3DiKTa** the ΔE_{ST} was found to be 0.21 eV and computed to be 0.26 eV.

2.4. Organic Light-Emitting Diodes

To evaluate the potential of **DiKTa** and **Mes_3DiKTa** in devices we fabricated several OLEDs, the two devices presented here are representative of the OLEDs tested (more device results are shown in Figures S27 and S28, Supporting Information). The device architecture was challenging as both emitters possess very deep HOMO levels. Thus, the difficulty to design these OLEDs arises from the very limited number of hosts with suitably deep HOMO levels. The optimized device structure was: ITO/HAT-CN (10 nm)/TAPC (40 nm)/TCTA (10 nm)/3.5 wt% emitter:mCP (20 nm)/TmPyPb (50 nm)/LiF (1 nm)/Al (100 nm) (**Figure 5**a), where indium tin oxide (ITO) is the anode, 1,4,5,8,9,11-hexaazatriphenylenehexacarbonitrile (HAT-CN) acts as the hole injection material, 4,4′-cyclohexylidenebis[*N*,*N*-bis(4-methylphenyl)benzenamine] (TAPC) and tris(4-carbazoyl-9-ylphenyl)amine (TCTA) act as hole transport layer, mCP is the host, 1,3,5-tri(*m*-pyridin-3-ylphenyl)benzene (TmPyPB) acts as electron-transporting material, and LiF modifies the work

Table 1. Solution lifetime data, rates, and efficiencies for DiKTa and Mes_3DiKTa in degassed dilute toluene at 300 K.

Compound	λ_{PL}[a] [nm]	FWHM[a] [nm] (cm^{-1})	Φ_{PL} (Φ_{DF})[b] [%]	τ_p, τ_d[c] [ns]; µs	$k_f/10^7$ s^{-1}	$k_{IC}/10^7$ s^{-1}	$k_{ISC}/10^7$ s^{-1}	Φ_{ISC} [%]	$k_{RISC}/10^4$ s^{-1}
DiKTa	453[d]	27 (1251)[d]	26 (1)	5.1; 23	4.9	14	0.75	3.8	4.6
Mes_3DiKTa	468[e]	29 (1306)[e]	37 (1)	6.7; 33	5.4	9.1	0.4	2.7	3.1

[a]In degassed toluene; [b]λ_{exc} = 360 nm; [c]λ_{exc} = 355 nm, prompt and delayed fluorescence were fitted as single exponential decays, shown in Figure S26 (Supporting Information); [d]λ_{exc} = 335 nm; [e]λ_{exc} = 345 nm.

Table 2. Thin film photophysical data at 3.5 wt% in mCP.

Compound	λ_{PL} [nm]	FWHM [nm] (cm^{-1})	Φ_{PL} [%]	τ_p; τ_d[a)] [ns]; µs	T_1[b)] [eV]	S_1[c)] [eV]	ΔE_{ST}[d)] [eV]
DiKTa	463[e)]	37 (1824)	75[f)]	4.4; 15	2.55	2.75	0.20
Mes_3DiKTa	477	37 (1689)	80	5.9; 20	2.46	2.67	0.21

[a)] λ_{exc} = 355 nm at 300 K under vacuum, prompt component obtained using a single exponential, delayed obtained using a stretched exponential; [b)]Obtained from the onset of the PL spectrum at 77 K after 70 ms, λ_{exc} = 415 nm; [c)]Obtained from the onset of the steady-state spectrum at 77 K, λ_{exc} = 335 nm; [d)]$\Delta E_{ST} = E(S_1) - E(T_1)$; [e)]Obtained at 300 K, λ_{exc} = 335 nm; [f)]Calculated using an integrating sphere, under N_2, λ_{exc} = 335 nm.

function of the aluminum cathode. The doping ratio was optimized at 3.5 wt% for both emitters as a function of Φ_{PL} and to avoid broadening FWHM due to aggregation formation as observed in **Mes_3DiKTa** devices with doping ratio ranging from 3.5% to 30% (Figure S28b, Supporting Information).

Both electroluminescence (EL) spectra are very narrow with FWHM of 39 and 36 nm (1848 and 1572 cm^{-1}), and associated CIE chromaticity coordinates of (0.14, 0.18) and (0.12, 0.32) for **DiKTa** and **Mes_3DiKTa**, respectively (Figure 5b). These EL spectra are significantly narrower than conventional blue D-A TADF OLEDs but similar to those EL spectra observed in R-TADF emitters (Table S5, Supporting Information). The EL spectra of our devices also showed very weak emission from the host at high voltages that likely occurs due to the slightly shallower HOMO level of mCP than the emitters (Figures S27a and S28a, Supporting Information).[20]

Figure 5d shows EQE versus luminance curves. The **DiKTa** OLED shows an EQE_{max} of 14.7% at 8 cd m^{-2} while the OLED

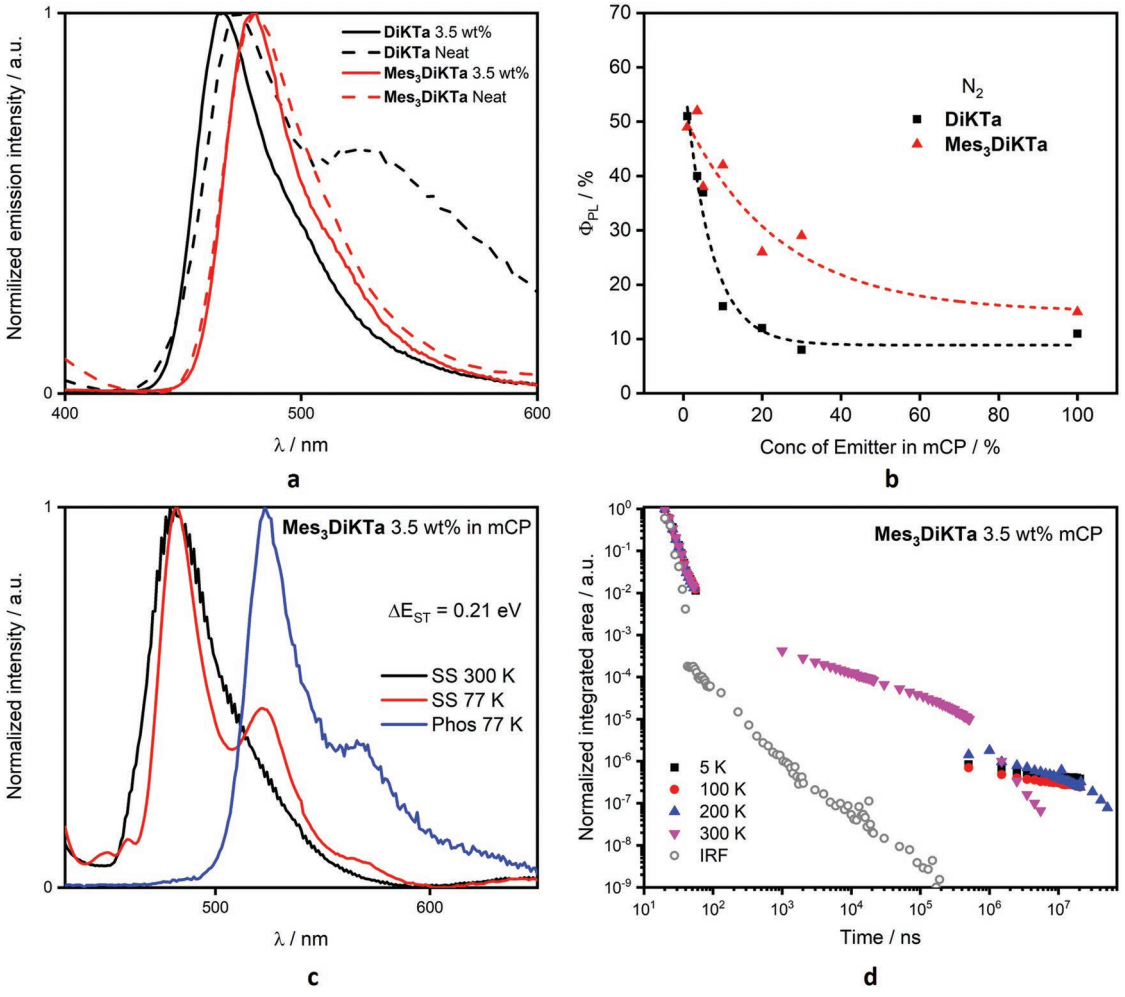

Figure 4. Solid-state effects of spin-coated films. a) Emission spectra at various concentrations at 300 K of **DiKTa** and **Mes_3DiKTa**. b) Varying PLQY at different concentrations **DiKTa** and **Mes3DiKTa** under N_2, λ_{exc} = 335 nm. The dashed line is a guide to the eye, based on fitting an exponential decay function to the data. c) Steady-state PL spectra at 300 K, at 77 K, and phosphorescence spectra in 3.5 wt% mCP, phosphorescence obtained at 77 K at a delay of 20 ms for 70 ms, λ_{exc} = 415 nm. d) Variable temperature time-resolved PL spectra, λ_{exc} = 355 nm in 3.5 wt% mCP, where IRF is the instrument response function.

Table 3. Device metrics for OLEDs employing **DiKTa** and **Mes$_3$DiKTa** and those of devices with similar literature emitters.

Emitter	V_{on}[a)] [V]	EQE_{max}[b)] [%]	Lum_{max}[c)] [cd m^{-2}]	EQE_{100}[d)] [%]	EQE_{1000}[d)] [%]	CIE (x,y)[e)]	FWHM[f)] [nm]	λ_{EL}[g)] [nm]	Ref.
DiKTa	≈3	14.7% at 8 cd m^{-2}	10 385	8.3	3.3	0.14,0.18	39	465	This work
Mes$_3$DiKTa	≈3	21.1% at 25 cd m^{-2}	12 949	14.5	4.5	0.12,0.32	36	480	This work
QAD (aka DiKTa)	N/A	19.4 at 0.2 cd m^{-2}	1100	9.4	1.4	0.13,0.18	39	468	[15]
3Ph-QAD	N/A	19.1 at 0.2 cd m^{-2}	4975	10.4	3.1	0.13,0.32	44	480	[16]
7Ph-QAD	N/A	18.7 at 0.2 cd m^{-2}	2944	5.4	2.1	0.12,0.24	34	472	[16]

[a)]V_{on} = Turn-on voltage; [b)]EQE = external quantum efficiency; [c)]Lum = luminance; [d)]Subscript 100 and 1000 refers to values taken at 100 cd m^{-2} and at 1000 cd m^{-2}, respectively; [e)]CIE = Internationale de L'Éclairage coordinates; [f)]FWHM = full width at half maximum; [g)]EL = electroluminescence.

with **Mes$_3$DiKTa** shows an EQE_{max} of 21.1% at 25 cd m^{-2}. Given these EQE_{max} values, the high Φ_{PL} of 80% and 75% in mCP and considering charge balance as 100% and outcoupling efficiency as 25%, the theoretical EQE_{max} for **DiKTa** and **Mes$_3$DiKTa** are ≈18% and ≈20%, respectively.[21] Thus, we can infer that essentially 100% of the triplet excitons are being efficiently harvested and converted to singlet excitons via the TADF mechanism. Though we must be careful, as there is some uncertainty on the efficiency of charge recombination and light extraction, this is a remarkable and somewhat unexpected result in view of the very low RISC rate in these molecules (see Table 1). It thus appears that, provided the triplets are protected against nonradiative loss mechanisms, a reasonably small ΔE_{ST} value as found in **DiKTa** and **Mes$_3$DiKTa** is enough to quantitatively upconvert

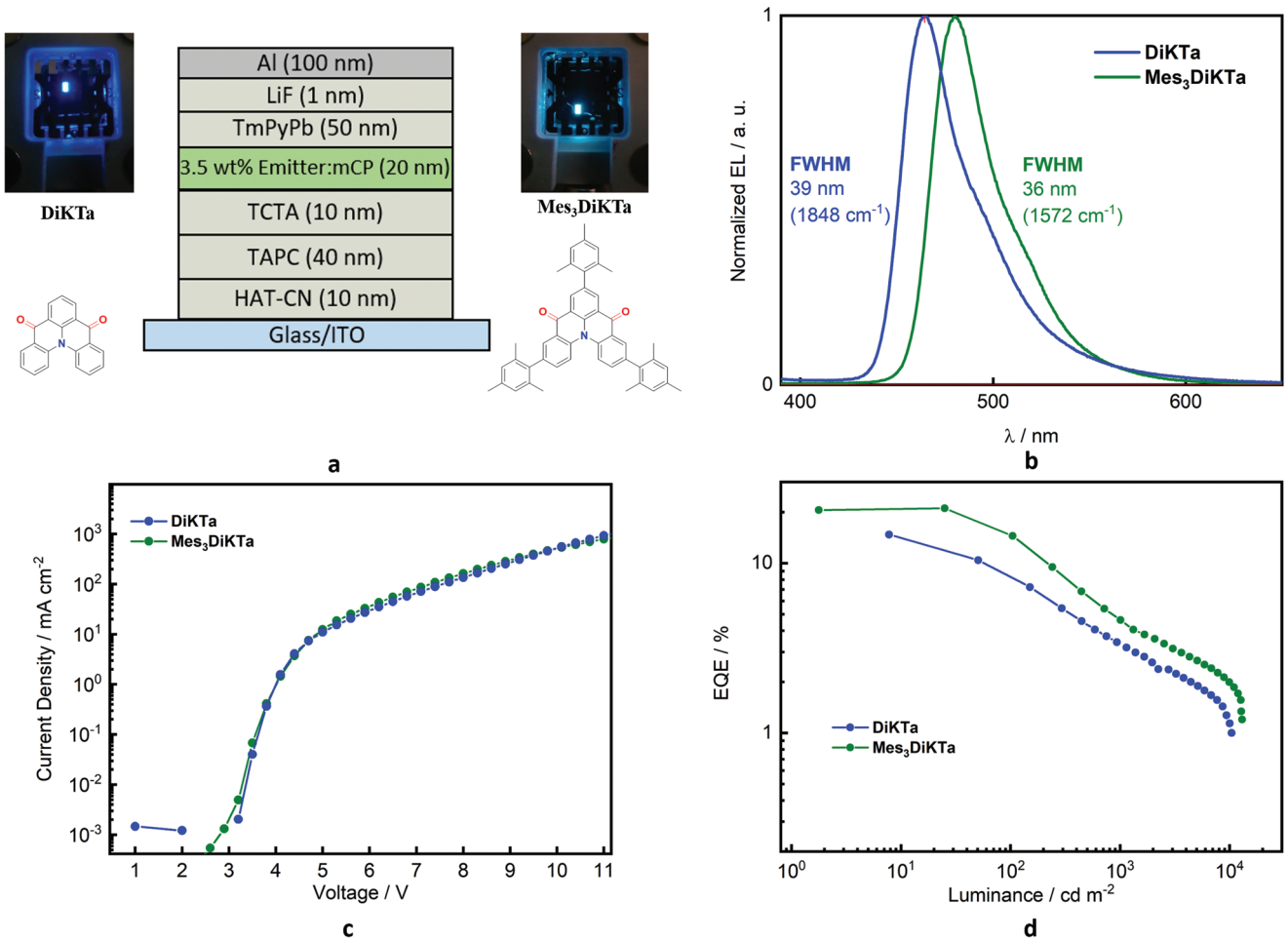

Figure 5. OLED data for **DiKTa** and **Mes$_3$DiKTa**. a) Device structure, b) electroluminescent spectra, c) current density versus voltage curves, and d) external quantum efficiencies (EQE) versus luminance.

all triplet excitations. We thus conclude that the weak coupling between the electronic excitations and the nuclei vibrations associated with the rigid backbone structure not only results in narrow spectral emission but also appears to slow down competitive nonradiative decay channels.

At 100 cd m^{-2} the EQE_{100} value for the OLED with **DiKTa** is 8.3%, decreasing 44% from its maximum value. The EQE_{100} for the device with **Mes_3DiKTa** is 14.5%, showing an efficiency roll-off of 31%. At 1000 cd m^{-2} the EQE_{1000} values decrease dramatically to 3.3% and 4.5% for **DiKTa** and **Mes_3DiKTa**, which is a decrease of 78% and 79% from their maximum values. This serious efficiency roll-off at high driving voltages was observed in other R-TADF emitters such as **DABNA-1** and **DABNA-2**,[5] and recently was also observed by Zhang and co-workers,[12] where **3-PhQAD** and **7-PhQAD** EQE values drop more than 85% from their maximum value at 1000 cd m^{-2}. Thus, we contend that the increased steric bulk afforded by the mesityl groups reduces the efficiency roll-off of the OLEDs when compared to **3-PhQAD** and **7-PhQAD**. Zhang and co-workers have investigated the mechanisms responsible for this strong efficiency roll-off and concluded that both triplet-triplet annihilation (TTA) and singlet exciton–polaron annihilation (SPA) play significant roles in the efficiency roll-off. Due to the similarity of **3-PhQAD** and **7-PhQAD** with our emitters and the similarity of the device structures, the cause of our efficiency roll-off is likely to be SPA and TTA as well. Even though the EQE values are poor at high driving voltages, the luminance levels reached by both emitters are excellent (Lum_{max} **DiKTa** = 10 400 cd m^{-2} and Lum_{max} **Mes_3DiKTa** = 13 000 cd m^{-2}), which is not often observed in TADF-based devices, including R-TADF OLED. Both devices operate at similar current densities and show low turn-on voltages of around 3 V (Figure S7c, Supporting Information). The previously reported OLEDs with **DiKTa**[15] using a similar device structure to the one used in this study showed EQE_{max} of 19.4% but at luminance lower than 1 cd m^{-2}. At comparable luminance of 10, 100, and 1000 cd m^{-2} they obtained similar EQE values of 15%, 9%, and 2% to those presented here. As such, **Mes_3DiKTa** demonstrated improved device performance in comparison to previously reported R-TADF materials, showing the highest EQE value at the relevant luminance of 100 cd m^{-2} among the keto R-TADF emitters reported to date (Table 3).

3. Conclusions

Based on a new molecular engineering approach to improve the efficiency of R-TADF emitters in OLEDs, we have designed the molecule **Mes_3DiKTa**. The OLED reached an EQE_{max} of up to 21%. When comparing **Mes_3DiKTa** to the parent **DiKTa** a ≈50% improvement in EQE_{max} is observed due to a significant reduction of aggregation-caused quenching by addition of mesityl groups to the resonant **DiKTa** core. By means of spin-component scaling second-order approximate coupled-cluster quantum-chemical calculations, we accurately predict ΔE_{ST}, with calculated values for **Mes_3DiKTa** being 0.26 eV compared to 0.21 eV determined experimentally in 3.5 wt% mCP. The modest ΔE_{ST} value originates from the nature of the involved electronic excitations that involve short-range reorganization in the electronic density offering simultaneously large singlet radiative decay rates and small singlet-triplet exchange interactions. Remarkably, despite a very slow reverse intersystem crossing process, all triplets upconvert into singlets in electroluminescence, a result that we ascribe to the rigid nature of the emitters. This leads to improved OLED device efficiency with reduced roll-off at luminance up to 100 cd m^{-2} without adversely affecting the R-TADF nature of the emitter. We further note that the improvement in device performance brought about by the use of peripherical side groups in **Mes_3DiKTa** has only a modest impact on the emission color, with CIE coordinates for blue emission similar to those measured for the **DiKTa** core. Finally, there is room for improvement at high luminance where efficiency roll-off remains large and we hope the strategy applied here can be further fine-tuned in the future to reduce bimolecular recombination, i.e., through the design of molecules with limited spectral overlap between singlet emission and charge and triplet absorption. Such work is currently in progress.

Supporting Information

Supporting Information is available from the Wiley Online Library or from the author. The research data supporting this publication can be accessed at https://doi.org/10.17630/e717a3b6-25b6-4bd8-b1aa-9459da244707.

Acknowledgements

This project has received funding from the European Union's Horizon 2020 research and innovation programme under the Marie Skłodowska Curie grant agreement No. 838885 (NarrowbandSSL). S.S. acknowledges support from the Marie Skłodowska-Curie Individual Fellowship. This work was funded by the EC through the Horizon 2020 Marie Sklodowska-Curie ITN project *TADF*life (grant #: 812872). The St Andrews team would also like to thank the Leverhulme Trust (RPG-2016-047) and EPSRC (EP/P010482/1) for financial support. Computational resources were provided by the Consortium des Équipements de Calcul Intensif (CÉCI), funded by the Fonds de la Recherche Scientifiques de Belgique (F.R.S.-FNRS) under Grant No. 2.5020.11, as well as the Tier-1 supercomputer of the Fédération Wallonie-Bruxelles, infrastructure funded by the Walloon Region under the Grant Agreement No. 1117545. A.P. acknowledges the financial support from the Marie Curie Fellowship (MILORD project, No. 748042). D.B. is a FNRS Research Director. The authors thank Franck-Julian Kahle for support with data analysis. Y.O. acknowledges fruitful discussions with Prof. Juan-Carlos Sancho-Garcia from the University of Alicante and Prof. Luca Muccioli from the University of Bologna.

Conflict of Interest

The authors declare no conflict of interest.

Keywords

blue emission, multiresonance thermally activated delayed fluorescence, organic light emitting diodes, SCS-CC2 approach

Received: September 27, 2019
Published online: December 3, 2019

[1] M. Y. Wong, E. Zysman-Colman, *Adv. Mater.* **2017**, *29*, 1605444.
[2] A. Endo, K. Sato, K. Yoshimura, T. Kai, A. Kawada, H. Miyazaki, C. Adachi, *Appl. Phys. Lett.* **2011**, *98*, 083302.
[3] A. Pershin, D. Hall, V. Lemaur, J. C. Sancho-Garcia, L. Muccioli, E. Zysman-Colman, D. Beljonne, Y. Olivier, *Nat. Commun.* **2019**, *10*, 597.
[4] H. Hirai, K. Nakajima, S. Nakatsuka, K. Shiren, J. Ni, S. Nomura, T. Ikuta, T. Hatakeyama, *Angew. Chem., Int. Ed.* **2015**, *54*, 13581.
[5] T. Hatakeyama, K. Shiren, K. Nakajima, S. Nomura, S. Nakatsuka, K. Kinoshita, J. Ni, Y. Ono, T. Ikuta, *Adv. Mater.* **2016**, *28*, 2777.
[6] a) X. Cai, S.-J. Su, *Adv. Funct. Mater.* **2018**, *28*, 1802558; b) M. Y. Wong, S. Krotkus, G. Copley, W. Li, C. Murawski, D. Hall, G. J. Hedley, M. Jaricot, D. B. Cordes, A. M. Z. Slawin, Y. Olivier, D. Beljonne, L. Muccioli, M. Moral, J. C. Sancho-García, M. C. Gather, I. D. W. Samuel, E. Zysman-Colman, *ACS Appl. Mater. Interfaces* **2018**, *10*, 33360; c) Y. Li, J.-Y. Liu, Y.-D. Zhao, Y.-C. Cao, *Mater. Today* **2017**, *20*, 258.
[7] S. Nakatsuka, H. Gotoh, K. Kinoshita, N. Yasuda, T. Hatakeyama, *Angew. Chem., Int. Ed.* **2017**, *56*, 5087.
[8] K. Matsui, S. Oda, K. Yoshiura, K. Nakajima, N. Yasuda, T. Hatakeyama, *J. Am. Chem. Soc.* **2018**, *140*, 1195.
[9] X. Liang, Z. P. Yan, H. B. Han, Z. G. Wu, Y. X. Zheng, H. Meng, J. L. Zuo, W. Huang, *Angew. Chem., Int. Ed.* **2018**, *57*, 11316.
[10] S. H. Han, J. H. Jeong, J. W. Yoo, J. Y. Lee, *J. Mater. Chem. C* **2019**, *7*, 3082.
[11] Y. Kondo, K. Yoshiura, S. Kitera, H. Nishi, S. Oda, H. Gotoh, Y. Sasada, M. Yanai, T. Hatakeyama, *Nat. Photonics* **2019**, *13*, 678.
[12] Y. J. Cho, S. K. Jeon, S.-S. Lee, E. Yu, J. Y. Lee, *Chem. Mater.* **2016**, *28*, 5400.
[13] J. Mei, N. L. C. Leung, R. T. K. Kwok, J. W. Y. Lam, B. Z. Tang, *Chem. Rev.* **2015**, *115*, 11718.
[14] a) J. E. Field, D. Venkataraman, *Chem. Mater.* **2002**, *14*, 962; b) J. E. Field, T. J. Hill, D. Venkataraman, *J. Org. Chem.* **2003**, *68*, 6071; c) S. K. Surampudi, G. Nagarjuna, D. Okamoto, P. D. Chaudhuri, D. Venkataraman, *J. Org. Chem.* **2012**, *77*, 2074.
[15] Y. Yuan, X. Tang, X.-Y. Du, Y. Hu, Y.-J. Yu, Z.-Q. Jiang, L.-S. Liao, S.-T. Lee, *Adv. Opt. Mater.* **2019**, *7*, 1801536.
[16] X. Li, Y.-Z. Shi, K. Wang, M. Zhang, C.-J. Zheng, D.-M. Sun, G.-L. Dai, X.-C. Fan, D.-Q. Wang, W. Liu, Y.-Q. Li, J. Yu, X.-M. Ou, C. Adachi, X.-H. Zhang, *ACS Appl. Mater. Interfaces* **2019**, *11*, 13472.
[17] V. V. Pavlishchuk, A. W. Addison, *Inorg. Chim. Acta* **2000**, *298*, 97.
[18] a) S. Haseyama, A. Niwa, T. Kobayashi, T. Nagase, K. Goushi, C. Adachi, H. Naito, *Nanoscale Res. Lett.* **2017**, *12*, 268; b) P. L. Santos, J. S. Ward, P. Data, A. S. Batsanov, M. R. Bryce, F. B. Dias, A. P. Monkman, *J. Mater. Chem. C* **2016**, *4*, 3815.
[19] S. A. Bagnich, A. Rudnick, P. Schroegel, P. Strohriegl, A. Kohler, *Philos. Trans. R. Soc., A* **2015**, *373*, 20140446.
[20] M.-S. Lin, S.-J. Yang, H.-W. Chang, Y.-H. Huang, Y.-T. Tsai, C.-C. Wu, S.-H. Chou, E. Mondal, K.-T. Wong, *J. Mater. Chem.* **2012**, *22*, 16114.
[21] M. C. Gather, S. Reineke, *Proc. SPIE* **2015**, *5*.